Quantitative phase-field modeling for dilute alloy solidification involving diffusion in the solid

Munekazu Ohno and Kiyotaka Matsuura
Division of Materials Science and Engineering, Graduate School of Engineering, Hokkaido University, North 13 West 8, Sapporo 060-8628, Japan
(Received 2 December 2008; published 5 March 2009)

An antitrapping current scheme for quantitative phase-field model [A. Karma, Phys. Rev. Lett. **87**, 115701 (2001)] is extended to solidification process in a dilute binary alloy system involving diffusion in the solid. It is demonstrated in an asymptotic analysis that in the case of an arbitrary value of the solid diffusivity, five types of constraints exist between interpolating functions used in the phase-field model, which need to be satisfied simultaneously to eliminate all anomalous interface effects. Then, the authors present an appropriate form of the antitrapping current term for the two-sided case to remove all the spurious effects. The convergence test of the output with respect to the interface thickness was carried out for the isothermal dendrite growth process, which demonstrates an excellent performance of the present model.

DOI: 10.1103/PhysRevE.79.031603 PACS number(s): 81.10.Aj, 81.30.Fb, 64.70.D−, 05.70.Ln

I. INTRODUCTION

The phase-field model has emerged as an effective computational tool to simulate a microstructural evolution process during phase transition [1]. Unique to the phase-field approach is the diffuse interface concept in which an interface is not a specific entity to be described separately, but is merely an inhomogeneous localization of the state variable called the "phase field." This allows one to avoid explicit tracking of moving phase boundaries in complex patterns, which is in marked contrast to computational methods based on a sharp-interface description [2]. The phase-field method has been applied to solidification processes for pure materials [3] and binary [4], multicomponent, and multiphase [5] alloy systems, demonstrating its capability of describing a variety of microstructural pattern formations.

The phase-field model for the solidification requires several phenomenological descriptions and assumptions to be introduced without addressing the underlying microscopic details of phenomena. Therefore, its output carries a quantitative meaning only when the model precisely reproduces the free-boundary problem of interest, more specifically, diffusion equation, mass conservation law at the interface, and the Gibbs-Thomson relation in the case of isothermal alloy solidification which is our main concern. In the so-called sharp-interface limit where the interface thickness W is taken to approach zero, the phase-field model is reduced to the free-boundary problem by holding a relation between measurable quantities and the parameter of the phase-field model [6]. However, such a sharp-interface limit model makes it virtually impossible to describe the phenomena on experimentally relevant spatial and temporal scales. This is because W, thus computational grid spacing Δx and the time constant for the simulation need to be quite small compared to the typical scales of the microstructural pattern to obtain a W-independent result [7]. Karma and Rappel demonstrated a seminal scheme to circumvent this serious deficit [8], focusing on the solidification of pure material with equal thermal diffusivities in the solid and liquid phases (symmetric model). They devised a model based on the thin-interface limit analysis in which the free-boundary problem is recovered with a finite value of W in the mesoscopic scale, showing the excellent computational performance of the model.

The thin-interface limit scheme has been extended to the alloy solidification process [9]. However, it has been pointed out that the thin-interface limit model of alloy solidification suffers from several deficiencies [10]. Almgren carried out a distinct thin-interface limit analysis for pure material with unequal diffusivities in the solid and liquid phases and demonstrated that in the case of asymmetric diffusivities, several anomalous effects exist which scale with W [10]. There are also analogous interface effects in the alloy solidification models, such as a discontinuity of the chemical potential across the interface (associated with abnormal solute trapping effect), solute diffusion along arclength of the interface (surface diffusion), and modification of the mass conservation condition at the interface due to interface stretching [10]. The elimination of these effects requires several constraints in interpolating functions used in the model to be satisfied simultaneously, which results in the stringent restriction on the model. It seems hardly possible to construct a computationally effective model which satisfies all the requirements only by elaborating appropriate forms of the interpolating functions. Karma devised a novel scheme to solve this problem in the case of the dilute alloy solidification with zero diffusivity in the solid (one-sided model) [11]. The essential ingredient in this scheme is a phenomenological antitrapping current term in the diffusion equation which is nonvanishing only in the interface region. This term provides an additional degree of freedom in choosing the interpolating functions, enabling the elimination of all the spurious effects for the one-sided model. This model is regarded as a quantitative phase-field model in that one can precisely describe the free-boundary problem with a computationally reasonable choice of W. This antitrapping current scheme has been increasingly utilized for quantitative computation of the solidification processes in dilute binary alloy [12–14] and has been extended to the multiphase system [15] and multicomponent system [16].

As mentioned, the significant progress has been made in the quantitative phase-field modeling for the alloy solidification. However, it should be pointed out that the antitrapping current scheme is, in a strict sense, validated only for the

one-sided system, viz., alloy with zero diffusivity in the solid. In most of alloy systems, the solid diffusivity is generally several orders of magnitude smaller than the liquid diffusivity. However, in the ferrite solidification of steel, one of the most important industrial alloys, the ratio of the diffusion coefficient in solid to the one in liquid is just order of $10^{-1}-10^{-2}$ [17]. Also, when an extremely slow cooling process is considered, the one-sided alloy model cannot reproduce the equilibrium process but inevitably describes the Scheil solidification process. In the multiphase system, moreover, the assumption of zero diffusivity in the solid prevents the diffusion controlled migration of solid-solid phase boundaries. This makes it virtually impossible to describe, for example, peritectic transformation process, which involves the solid-solid diffusion as well as liquid-solid diffusion to complete the transformation. Despite these facts, little has been addressed regarding the quantitative phase-field modeling for the system with arbitrary value of the solid diffusivity. The extension of the antitrapping current scheme to the two-sided model has been attempted in Ref. [18]. The authors demonstrated a thin-interface limit analysis and discussed a possible form of the antitrapping current term for the two-sided model. However, the performance of their model has not been clarified with thorough convergence tests. Importantly, their antitrapping current term has a singularity in the one-sided case, that is, the contribution of this term becomes divergently large when the solid diffusivity becomes quite small, which is inconsistent with the originally developed phase-field model for the one-sided system [11,12]. Such a divergently large contribution in the solute current may lead to a computational difficulty. In this regard, it is considered that the quantitative phase-field modeling has not been successfully generalized to the system with an arbitrary value of solid diffusivity. A gap between the models still exists for one-sided and symmetric cases and such a gap should be appropriately bridged by a generalized model for two-sided case.

The main objective of the present study is to develop a quantitative phase-field model for dilute alloy solidification with arbitrary value of solid diffusivity. For this, we extend the antitrapping current scheme to the two-sided case and demonstrate the antitrapping current term which enables elimination of all the spurious interface effects. It will be seen that the present model is precisely reduced to the previously developed symmetric and one-sided models as special cases. The performance of the present model is investigated in terms of the convergence test of the solution with respect to the interface thickness, focusing on isothermal dendrite growth.

The organization of this paper is as follows. First, we specify the free-boundary problem of our interest in the next section and discuss a general form of the phase-field model in Sec. III, which is a starting point of the present modeling. For clear exposition of the problem, in Sec. IV, we demonstrate the matched asymptotic analysis for the two-sided model where the antitrapping current term is introduced. The detail of the matched asymptotic analysis for one-sided model was reported in Ref. [12] and our analysis corresponds to the extension of their analysis to the two-sided case. Then, we present the phase-field model with nonzero solid diffusivity which is free from the anomalous effects in Sec. V. Since lengthy explanation is devoted to mathematical derivation of the present modeling in Secs. IV and V, we summarize only the essential equations of the present model required for computation in Sec. VI. The performance of this model is discussed in Sec. VII, followed by the conclusion in the final section.

II. FREE-BOUNDARY PROBLEM FOR ISOTHERMAL SOLIDIFICATION

In this section, we specify the free-boundary problem of our interest which forms a basis in the matched asymptotic analysis given in Sec. IV. We shall consider the solidification process of a dilute binary alloy consisting of elements A and B with liquidus slope m and the partition coefficient k. Provided that the local equilibrium condition is satisfied at the interface, the concentration of element B at the solid side of the interface c_s^* is given as $c_s^*=kc_l^*$ with the concentration of element B at the liquid side of the interface c_l^*. The temperature at the interface satisfies the following Gibbs-Thomson relation:

$$T = T_m - |m|c_l^* - \Gamma\tilde{\kappa} - V_n/\mu, \tag{2.1}$$

where T_m is the melting temperature of pure material A and Γ is the Gibbs-Thomson coefficient given as $\Gamma=\gamma\cdot T_m/\Delta H$ with surface tension γ and the latent heat of fusion per unit volume ΔH. For simplicity, we do not take into account the anisotropy of the surface tension in this section and also in the thin-interface limit analysis of Sec. IV. In Eq. (2.1), $\tilde{\kappa}$ is the interface curvature, V_n is the normal velocity of the interface, and μ is the linear kinetic coefficient. For the isothermal solidification at a temperature T_0, the Gibbs-Thomson relation is rewritten as

$$c_l^*/c_l^e = 1 - (1-k)d_0\tilde{\kappa} - (1-k)\tilde{\beta}V_n, \tag{2.2}$$

where c_l^e is the equilibrium concentration of the liquid at T_0, expressed as $c_l^e=(T_m-T_0)/|m|$. d_0 is the chemical capillary length given as

$$d_0 = \Gamma/\Delta T_0, \tag{2.3}$$

where $\Delta T_0=|m|(1-k)c_l^e$ is the solidification range. $\tilde{\beta}$ in Eq. (2.2) is defined as $\tilde{\beta}=1/(\mu\Delta T_0)$. In the bulk phase, the concentration c obeys the diffusion equation

$$\partial_t c = D_i\nabla^2 c, \tag{2.4}$$

where ∂_t represents time derivative, D_i is the diffusion coefficient and its subscript i with $i=s$, and l distinguishes the solid and liquid phases, respectively. In addition, the following condition should be satisfied to assure the mass conservation at the interface:

$$c_l^*(1-k)V_n = D_s\partial_n c|^- - D_l\partial_n c|^+, \tag{2.5}$$

where $\partial_n c|^-$ and $\partial_n c|^+$ are the spatial derivatives of the concentration normal to the interface at the solid and liquid sides of the interface, respectively.

For the convenience in the discussion, we introduce the dimensionless local supersaturation u as follows:

$$u = \frac{c/j_{\pm} - c_l^e}{c_l^e(1-k)}, \tag{2.6}$$

with $j_+=1$ in the bulk liquid phase and $j_-=k$ in the solid phase. Utilizing this dimensionless quantity u, Eqs. (2.2), (2.4), and (2.5), are rewritten as

$$u^* = -d_0\tilde{\kappa} - \tilde{\beta}V_n, \tag{2.7}$$

$$\partial_t u = D_i \nabla^2 u, \tag{2.8}$$

$$[1+(1-k)u^*]V_n = kD_s\partial_n u|^- - D_l\partial_n u|^+, \tag{2.9}$$

where u^* represents the value at the interface. The matched asymptotic analysis in Sec. IV is carried out in the light of the free-boundary problem thus described.

III. PHASE-FIELD MODEL

In this section, we start with a general form of the phase-field model for the alloy solidification based on the Kim-Kim-Suzuki (KKS) model [9]. It is first shown that in a dilute solution system, the thermodynamic model given in Refs. [11–13] is essentially equivalent to the KKS model.

As in the previous section, we shall consider the isothermal solidification in the dilute binary alloy system consisting of elements A and B with liquidus slope m and partition coefficient k. We introduce the phase field p specifying the solid phase with $p=1$ and the liquid phase with $p=0$. The interface is defined as a mixture of the solid and liquid phases [9]. The Ginzburg-Landau-type free energy functional of the system is given as follows:

$$F = \int_V \{(\tilde{\sigma}^2/2)(\nabla p)^2 + \tilde{\omega}\tilde{f}(p) + \tilde{g}(p)f_s + [1-\tilde{g}(p)]f_l\}dV, \tag{3.1}$$

where $\tilde{\sigma}$ is the gradient energy coefficient, $\tilde{f}(p)$ is the double-well potential with minima at $p=1$ and 0, and $\tilde{\omega}$ is the potential height. f_s and f_l are the free energy densities for the bulk solid and liquid, respectively. The interpolating function $\tilde{g}(p)$ is a monotonous function satisfying $\tilde{g}(0)=0$ and $\tilde{g}(1)=1$.

The two concentration fields for the solid c_s and for the liquid c_l are introduced. In the interfacial region, these concentrations obey the mixture rule $c=\tilde{h}(p)c_s+[1-\tilde{h}(p)]c_l$ with an interpolating function $\tilde{h}(p)$. The concentrations c_s and c_l are not independent of each other and the relation between them is determined by the condition of equal chemical potentials at each point $\partial f_s/\partial c_s = \partial f_l/\partial c_l = \mu_c$ which is the essential condition introduced in the KKS model [9]. This condition allows the equilibrium phase field profile to be decoupled from the concentration profile, removing an extra contribution to the surface energy which depends on the solute concentration at the interface and the temperature. In the present study, we hold a relation $c_s=kc_l$, since our focus is placed on the dilute solution system. Then, the tempora l evolution of the phase field p can be described by the time-dependent Ginzburg-Landau equation $\partial_t p = -\tilde{M}\delta F/\delta p$ with the phase-field mobility $\tilde{M}$, which is explicitly given as [9]

$$\tilde{M}^{-1}\partial_t p = \tilde{\sigma}^2\nabla^2 p - \tilde{\omega}\tilde{f}' - \tilde{g}'[f_s(c_s) - f_l(c_l) - (c_s - c_l)\mu_c], \tag{3.2}$$

where $\tilde{f}' = d\tilde{f}/dp$ and $\tilde{g}' = d\tilde{g}/dp$. The time evolution of the concentration field is described by the following diffusion equation:

$$\partial_t c = \nabla D(p)\{\tilde{h}(p)\nabla c_s + [1-\tilde{h}(p)]\nabla c_l\}, \tag{3.3}$$

where $D(p)$ is the diffusivity of the phase field dependent with $D(1)=D_s$ and $D(0)=D_l$. It is noted that the function $\tilde{h}(p)$ should be equivalent to $\tilde{g}(p)$ in the variational formulation. On the other hand, these two functions are independently defined within a nonvariational formulation and this allows a simple choice of $h(p)=p$, which is advantageous in terms of the computational efficiency [8]. In the following, our discussion is given in the nonvariational form, though it is applicable to the case of the variational formulation.

The relation between the KKS model and the other models given in Refs. [11–13] can readily be grasped by transforming the variables. For this, we introduce the phase field ϕ given as $\phi=2p-1$. The solid and liquid phases are specified by $\phi=+1$ and -1, respectively. Furthermore, the dimensionless local supersaturation u is defined as

$$u = \frac{c_l - c_l^e}{c_l^e - c_s^e}. \tag{3.4}$$

This is equivalent to the definition of Eq. (2.6) in the sharp-interface description. In the dilute solute limit, the thermodynamic driving force in Eq. (3.2) can be approximated as [9]

$$f_s(c_s) - f_l(c_l) - (c_s - c_l)\mu_c \approx -\frac{RT_0}{v_m}[c_l^e - c_s^e - (c_l - c_s)] \approx -\frac{RT_m}{v_m}[c_l^e - c_s^e - (c_l - c_s)], \tag{3.5}$$

where R is the gas constant and v_m is the molar volume. In this approximation, we neglect mc_l^e term in $T_0=T_m-mc_l^e$, since this term results in the second-order contribution of concentration which is negligibly small in the dilute solution limit. Then, Eqs. (3.2) and (3.3) are rewritten in terms of ϕ and u introducing the antitrapping current term j_{AT},

$$M^{-1}\partial_t\phi = \sigma^2\nabla^2\phi - \omega 2\tilde{f}' - \tilde{g}'\lambda u, \tag{3.6}$$

$$\frac{[1+k-(1-k)h(\phi)]}{2}\partial_t u = \nabla[D_l q(\phi)\nabla u - j_{\mathrm{AT}}] + \frac{1}{2}[1+(1-k)u]\partial_t h(\phi), \tag{3.7}$$

where $M=4\tilde{M}$, $\sigma=\tilde{\sigma}/2$, $\omega=\tilde{\omega}/4$, and λ is given as $\lambda=RT_m(1-k)(c_l^e-c_s^e)/(2v_m)$ and $h(\phi)=2\tilde{h}(\phi)-1$. $q(\phi)$ is represented by

$$q(\phi)=\frac{D(\phi)}{D_l}\frac{[1+k-(1-k)h(\phi)]}{2} \tag{3.8}$$

and, accordingly, $q(+1)=kD_s/D_l$ and $q(-1)=1$. The antitrapping current term j_{AT} is given as [12]

$$j_{\mathrm{AT}}=-a(\phi)\frac{\sigma}{\sqrt{\omega}}[1+(1-k)u]\partial_t\phi\frac{\nabla\phi}{|\nabla\phi|}. \tag{3.9}$$

This is a phenomenologically introduced term which is nonvanishing only in the interface region. $a(\phi)$ is an interpolating function which provides an additional degree of freedom in choosing a set of the interpolating functions. When we further define $\tau=(M\omega)^{-1}$, $W^2=\sigma^2\omega^{-1}$, $\lambda^*=(15/8)\lambda/\omega$, $f'=2\tilde{f}'$, and $g'=(8/15)\tilde{g}'$, Eqs. (3.6) and (3.7) are, respectively, expressed as

$$\tau\partial_t\phi=W^2\nabla^2\phi-f'(\phi)-\lambda^*g'(\phi)u, \tag{3.10}$$

$$\frac{[1+k-(1-k)h(\phi)]}{2}\partial_t u=\nabla\left(D_l q(\phi)\nabla u+a(\phi)W[1+(1-k)u]\partial_t\phi\frac{\nabla\phi}{|\nabla\phi|}\right)+\frac{1}{2}[1+(1-k)u]\partial_t h(\phi). \tag{3.11}$$

Equations (3.10) and (3.11) represent the final set of equations for the present phase-field model. When we consider one-dimensional profile of ϕ during steady state with boundary condition $\phi=1$ at $x\to-\infty$ and $\phi=-1$ at $x\to+\infty$, this model leads to $\phi_e(x)=-\tanh[x/(\sqrt{2}W)]$. It should be noted that W corresponds to a measure of the thickness of the diffuse interface. Also, the surface tension γ is represented by

$$\gamma=IW\omega, \tag{3.12}$$

where $I=2\sqrt{2}/3$. As the advantage of the KKS model, γ does not depend on the solute concentration field.

It is important to point out that Eqs. (3.10) and (3.11) are identical to Eqs. (68) and (69) in Ref. [12] except for the fact that our discussion is limited to the isothermal process. Also, the model of Ref. [10] for a pure material, where a thin-interface limit analysis was performed in the case of a two-sided model, is regarded as a special case of the above equations with $k=1$ and $a(\phi)=0$. In the following, we present the thin-interface limit analysis of Eqs. (3.10) and (3.11).

IV. ASYMPTOTIC ANALYSIS FOR TWO-SIDED MODEL

In this section, we carry out the matched asymptotic analysis of the phase-field model given by Eqs. (3.10) and (3.11) in order to demonstrate the constraints imposed on the model for description of the free-boundary problem. As already mentioned, the asymptotic analysis for the one-sided model with the antitrapping current term was detailed in Ref. [12]. The present analysis corresponds to the extension of their analysis to the case of the two-sided model. We use an expansion parameter $\varepsilon=W/d_0$ and perform the asymptotic analysis up to second order in ε. As pointed out in Ref. [12], this expansion scheme with ε yields all important correction terms at second order.

A. Dimensionless expressions and matching conditions

It is first convenient to rewrite the sharp-interface model and the phase-field model in dimensionless forms by measuring length in unit of d_0 and time in unit of d_0^2/D_l. Using these dimensionless spatial and time scales, the sharp-interface equations (2.7)–(2.9) are rewritten as

$$\partial_t u=q_i\nabla^2 u \text{ with } i=s \text{ or } l, \tag{4.1}$$

where $q_s=D_s/D_l=q(+1)/k$ for the solid, $q_l=q(-1)$ for the liquid, and

$$u^*=-\kappa-\beta v_n, \tag{4.2}$$

$$[1+(1-k)u^*]v_n=q(+1)\partial_n u|^--q(-1)\partial_n u|^+, \tag{4.3}$$

where $\kappa=d_0\tilde{\kappa}$ is the dimensionless interface curvature, $\beta=\tilde{\beta}D_l/d_0$ is the dimensionless kinetic coefficient, and $v_n=d_0V_n/D_l$ is the dimensionless normal velocity.

In the phase-field model, we first utilize the van't Hoff relation for the dilute binary alloy given by $m=T_m^2R(1-k)/(v_m\Delta H)$ to express λ^* as

$$\lambda^*=\frac{15}{8}\frac{RT_m}{2v_m\omega}(1-k)(c_l^e-c_s^e)=\frac{15}{8}\frac{m\Delta H}{2T_m\omega}(c_l^e-c_s^e)=\frac{15}{16}\frac{IW}{d_0}=a_1\varepsilon, \tag{4.4}$$

where $a_1=I/J$ with $J=g(+1)-g(-1)=16/15$. Then, the dimensionless forms of the phase field model are given by

$$\alpha\varepsilon^2\partial_t\phi=\varepsilon^2\nabla^2\phi-f'(\phi)-a_1\varepsilon g'(\phi)u, \tag{4.5}$$

$$\frac{[1+k-(1-k)h(\phi)]}{2}\partial_t u=\nabla\left(q(\phi)\nabla u+a(\phi)\varepsilon[1+(1-k)u]\partial_t\phi\frac{\nabla\phi}{|\nabla\phi|}\right)+\frac{1}{2}[1+(1-k)u]\partial_t h(\phi), \tag{4.6}$$

where $\alpha=D_l\tau/W^2$.

In the following, we will expand the ϕ and u fields in power of ε. In order to avoid an expected abrupt variation of these fields along the interface, one needs to deal with the solutions in two regions [19]; an inner region which corresponds to the spatially diffuse interface region where ϕ varies rapidly and an outer region which represents the bulk phase region away from the interface. The expansions in the inner region will be matched order by order in power of ε to those in the outer region. The outer and inner expansions of the phase field are written as $\Phi=\Phi_0+\varepsilon\Phi_1+\varepsilon^2\Phi_2+\cdots$ and

$\phi=\phi_0+\varepsilon\phi_1+\varepsilon^2\phi_2+\cdots$, respectively. Similarly, the outer and inner expansions of the u field are given as $U=U_0+\varepsilon U_1+\varepsilon^2 U_2+\cdots$ and $u=u_0+\varepsilon u_1+\varepsilon^2 u_2+\cdots$, respectively. Since in the outer region Φ is constant in each phase and $g'(\pm 1)=0$, $\Phi=\pm 1$ are stable solutions for the ϕ equation (4.5) to all orders in ε for any value of U. Accordingly, $U_{n'}$ simply obeys the diffusion equation to all orders in ε

$$\partial_t U_{n'} = q_i \nabla^2 U_{n'} \text{ with } n' = 0,1,2,\ldots, \tag{4.7}$$

where $i=s$ in the solid and $i=l$ in the liquid.

In order to find the inner solution, as described in Refs. [8,12], we rewrite the phase-field equations (4.5) and (4.6) in terms of a local orthogonal set of curvilinear coordinates in the reference frame of the interface r (signed distance to the $\phi=0$ level set) and s (arclength along the interface) and then the rescaled coordinate $\eta=r/\varepsilon$. The detail of the differential operators in terms of r and s is found in Refs. [12,19]. In this coordinate system, the phase-field equations are expressed as [12]

$$\begin{aligned}&\partial_\eta{}^2\phi - f'(\phi) + \varepsilon[(\alpha v_n+\kappa)\partial_\eta\phi - a_1 g'(\phi)u] \\ &\quad + \varepsilon^2(\partial_s{}^2\phi - \kappa^2\eta\partial_\eta\phi) = O(\varepsilon^3),\end{aligned} \tag{4.8}$$

$$\begin{aligned}&\varepsilon^{-2}\partial_\eta[q(\phi)\partial_\eta u] + \varepsilon^{-1}\Big(\tfrac{1}{2}v_n[1+k-(1-k)h(\phi)](\partial_\eta u) \\ &\quad - \tfrac{1}{2}v_n[1+(1-k)u]\partial_\eta h(\phi) + v_n\partial_\eta\{a(\phi)[1+(1-k)u] \\ &\quad \times(\partial_\eta\phi)\} + \kappa q(\phi)\partial_\eta u\Big) + \kappa v_n a(\phi)[1+(1-k)u](\partial_\eta\phi) \\ &\quad - \kappa^2\eta q(\phi)\partial_\eta u + \partial_s[q(\phi)\partial_s u] = O(\varepsilon).\end{aligned} \tag{4.9}$$

As mentioned, the expansions in the inner region will be matched order by order in power of ε to those in the outer region. The matching conditions for the phase field are trivial as given by

$$\phi_0(\eta,s) = \mp 1 \text{ as } \eta \to \pm\infty,$$

$$\phi_{n'}(\eta,s) = 0 \text{ as } \eta \to \pm\infty, \tag{4.10}$$

with $n' \geqslant 1$. The matching conditions for u field are exemplified as [12]

$$u_0(\eta,s) = U_0|^{\pm}(s) \text{ as } \eta \to \pm\infty,$$

$$u_1(\eta,s) = U_1|^{\pm}(s) + \eta\partial_r U_0|^{\pm}(s) \text{ as } \eta \to \pm\infty,$$

$$\begin{aligned}u_2(\eta,s) = {}& U_2|^{\pm}(s) + \eta\partial_r U_1|^{\pm}(s) + (\eta^2/2)\partial_r^2 U_0|^{\pm}(s) \\ & \text{as } \eta \to \pm\infty,\end{aligned} \tag{4.11}$$

where $C|^{\pm}$ represents the quantity C evaluated at the interface, approaching from the liquid side ($C|^{+}$) or the solid side ($C|^{-}$).

B. ϕ equation at ε^0

Substituting the inner expansion of the phase field into Eq. (4.8), we obtain at the leading order

$$\partial_\eta{}^2\phi_0 - f'(\phi_0) = 0. \tag{4.12}$$

When we define $f'(\phi_0)=-\phi_0+\phi_0{}^3$, this relation yields

$$\phi_0(\eta) = -\tanh\frac{\eta}{\sqrt{2}} \tag{4.13}$$

with the matching condition (4.10). Also, we can grasp the relation $\partial_\eta\phi_0=(1/\sqrt{2})(\phi_0{}^2-1)$.

C. u equation at ε^{-2}

The substitution of the inner expansion of the u field into Eq. (4.9) yields at order ε^{-2},

$$\partial_\eta[q(\phi_0)\partial_\eta u_0] = 0, \tag{4.14}$$

of which the integration once leads to $\partial_\eta u_0=C_0(s)/q(\phi_0)$. From the matching condition (4.11), we have the condition $\lim_{\eta\to\pm\infty}\partial_\eta u_0(\eta,s)=0$. Thus, $C_0(s)=0$ and

$$u_0(\eta,s) = \bar{u}_0(s). \tag{4.15}$$

It is seen that u_0 is independent of η and is continuous across the interface.

D. ϕ equation at ε^1

The phase-field equation (4.8) at the first order in ε is written as

$$L\phi_1 = a_1 g'(\phi_0)u_0 - (\alpha v_n+\kappa)\partial_\eta\phi_0, \tag{4.16}$$

where $L=\partial_\eta{}^2-f''(\phi_0)$ is a linear differential operator. It is noted that the partial derivative of Eq. (4.12) with respect to η yields the relation $L\partial_\eta\phi_0=0$. Since L is the self-adjoint, the right-hand side of Eq. (4.16) must be orthogonal to $\partial_\eta\phi_0$, which leads to

$$a_1 u_0 J + (\alpha v_n+\kappa)I = 0, \tag{4.17}$$

where

$$J = -\int_{-\infty}^{+\infty} g'(\phi_0)\partial_\eta\phi_0 d\eta = g(+1) - g(-1), \tag{4.18}$$

$$I = \int_{-\infty}^{+\infty} (\partial_\eta\phi_0)^2 d\eta. \tag{4.19}$$

The constants I and J are the same as those employed in Eq. (4.4). Therefore, we arrive at the following Gibbs-Thomson condition:

$$\bar{u}_0 = -\alpha v_n - \kappa, \tag{4.20}$$

which becomes identical to Eq. (4.2) by holding $\beta=\alpha$.

E. u equation at ε^{-1}

$$\begin{aligned}\partial_\eta[q(\phi_0)\partial_\eta u_1] = {}& \tfrac{1}{2}v_n[1+(1-k)\bar{u}_0]\partial_\eta h(\phi_0) - v_n\partial_\eta\{a(\phi_0) \\ & \times[1+(1-k)\bar{u}_0](\partial_\eta\phi_0)\}.\end{aligned} \tag{4.21}$$

We integrate this equation once to find

$$q(\phi_0)\partial_\eta u_1 = \tfrac{1}{2}v_n'[h(\phi_0) - 2a(\phi_0)(\partial_\eta\phi_0)] + A_1(s), \tag{4.22}$$

with $v_n'=v_n[1+(1-k)\bar{u}_0]$ and an integral constant A_1, and second time to obtain

$$u_1 = \frac{1}{2}v_n' \int_0^\eta \frac{[h(\phi_0) - 2a(\phi_0)(\partial_\xi \phi_0)]}{q(\phi_0)} d\xi + \int_0^\eta \frac{A_1(s)}{q(\phi_0)} d\xi + A_2(s), \tag{4.23}$$

with constant A_2. Thus, the matching condition (4.11) leads to

$$u_1 = A_2(s) + A_1(s)G_\pm + \frac{v_n'}{2}F_\pm + \left\{ \frac{A_1(s)}{q(\mp 1)} + \frac{v_n'}{2}p(\mp 1) \right\} \eta = U_1|^\pm + \eta \partial_r U_0|^\pm \quad \text{as } \eta \to \pm\infty, \tag{4.24}$$

where

$$G_\pm = \int_0^{\pm\infty} \left(\frac{1}{q(\phi_0)} - \frac{1}{q(\mp 1)} \right) d\eta, \tag{4.25}$$

$$F_\pm = \int_0^{\pm\infty} [p(\phi_0) - p(\mp 1)] d\eta, \tag{4.26}$$

$$p(\phi_0) = [h(\phi_0) - 2a(\phi_0)(\partial_\eta \phi_0)]/q(\phi_0). \tag{4.27}$$

Since the term $a(\phi_0)\partial_\eta \phi_0$ vanishes at the limit $\eta \to \pm\infty$, we have $p(\mp 1) = \mp 1/q(\mp 1)$. Therefore, we obtain

$$\partial_r U_0|^\pm = \frac{A_1(s)}{q(\mp 1)} \mp \frac{v_n'}{2q(\mp 1)} \tag{4.28}$$

and, also,

$$A_1(s) = \tfrac{1}{2}q(-1)\partial_r U_0|^+ + \tfrac{1}{2}q(+1)\partial_r U_0|^-, \tag{4.29}$$

$$[1 + (1-k)\bar{u}_0]v_n = q(+1)\partial_r U_0|^- - q(-1)\partial_r U_0|^+. \tag{4.30}$$

It should be noted that Eq. (4.30) is the leading order expression of the mass conservation law at the interface. From Eq. (4.24), we furthermore find

$$U_1|^+ - U_1|^- = A_1(s)(G_+ - G_-) + \frac{v_n'}{2}(F_+ - F_-). \tag{4.31}$$

Hence, in order for U_1 to be continuous across the interface, it is necessary to satisfy the following conditions:

$$G_+ = G_- = \tilde{G}, \tag{4.32}$$

$$F_+ = F_- = \tilde{F}. \tag{4.33}$$

These are the integral constraints between $q(\phi)$, $a(\phi)$, and $h(\phi)$.

F. ϕ equation at ε^2

$$L\phi_2 = \frac{f'''(\phi_0)}{2}{\phi_1}^2 - (\alpha v_n + \kappa)\partial_\eta \phi_1 + a_1 g'(\phi_0)u_1 + a_1 \bar{u}_0 g''(\phi_0)\phi_1 + \kappa^2 \eta \partial_\eta \phi_0. \tag{4.34}$$

From the discussion given in Eq. (4.16), one can realize that the left-hand side of Eq. (4.34) be vanished by multiplying $\partial_\eta \phi_0$ and integrating it from $-\infty$ to $+\infty$. As for the right-hand side of Eq. (4.34), the symmetry properties of the involved functions are utilized as in Refs. [8,12]. The substitution of Eq. (4.20) into Eq. (4.16) yields

$$L\phi_1 = -(\alpha v_n + \kappa)[a_1 g'(\phi_0) + \partial_\eta \phi_0], \tag{4.35}$$

where L is the even operator and $\partial_\eta \phi_0$ is the even function. Since $g(\phi)$ is chosen so that $g(1) = -g(-1)$, g' is even in η. Therefore, ϕ_1 is an even function and $\partial_\eta \phi_1$ is an odd function. In the right-hand side of Eq. (4.34), ${\phi_1}^2$, $g'(\phi_0)$, and $\partial_\eta \phi_0$ are even functions, while $f'''(\phi_0)$, $\partial_\eta \phi_1$ and g'' are odd functions. From Eq. (4.34), then, one realizes the following relation to be held:

$$a_1 \int_{-\infty}^{+\infty} g'(\phi_0) u_1 \partial_\eta \phi_0 d\eta = 0. \tag{4.36}$$

The substitution of Eq. (4.23) into Eq. (4.36) leads to

$$\frac{1}{2}v_n' \int_{-\infty}^{+\infty} \left(\int_0^\eta p(\phi_0) d\xi \right) g'(\phi_0)\partial_\eta \phi_0 d\eta + \int_{-\infty}^{+\infty} \left(\int_0^\eta \frac{A_1(s)}{q(\phi_0)} d\xi \right) g'(\phi_0)\partial_\eta \phi_0 d\eta - JA_2(s) = 0. \tag{4.37}$$

The second term in Eq. (4.37) can be transformed as

$$\begin{aligned} &\int_{-\infty}^{+\infty} \left(\int_0^\eta \frac{A_1(s)}{q(\phi_0)} d\xi \right) g'(\phi_0)\partial_\eta \phi_0 d\eta \\ &= \int_{-\infty}^{+\infty} \left(\int_0^\eta \frac{A_1(s)}{q(\phi_0)} d\xi \right) \frac{dg(\phi_0)}{d\eta} d\eta \\ &= A_1(s) \int_0^{+\infty} \frac{g(-1) - g(\phi_0)}{q(\phi_0)} d\eta - A_1(s) \int_0^{-\infty} \frac{g(+1) - g(\phi_0)}{q(\phi_0)} d\eta \\ &= A_1(s)g(-1)G_+ - A_1(s)g(+1)G_- + A_1(s)(\hat{F}_+ - \hat{F}_-), \end{aligned} \tag{4.38}$$

where

$$\hat{F}_\pm = \int_0^{\pm\infty} \left(\frac{g(\mp 1)}{q(\mp 1)} - \frac{g(\phi_0)}{q(\phi_0)} \right) d\eta. \tag{4.39}$$

Accordingly, provided that the condition given by Eq. (4.32) is satisfied, we can determine the constant $A_2(s)$ as follows:

$$A_2(s) = -A_1(s)\tilde{G} + \frac{A_1(s)}{J}(\hat{F}_+ - \hat{F}_-) + \frac{1}{2}v_n' \frac{\tilde{K}}{J}, \tag{4.40}$$

where

$$\tilde{K} = \int_{-\infty}^{+\infty} \left(\int_0^{\eta} p(\phi_0) d\xi \right) g'(\phi_0) \partial_\eta \phi_0 d\eta. \tag{4.41}$$

Substituting Eq. (4.40) into Eq. (4.24), we realize the following relation:

$$U_1|^{\pm} = A_2(s) + A_1(s)\tilde{G} + \frac{v_n'}{2}\tilde{F}$$

$$= \frac{A_1(s)}{J}(\hat{F}_+ - \hat{F}_-) + \frac{1}{2}v_n' \left(\frac{\tilde{K} + J\tilde{F}}{J} \right), \tag{4.42}$$

where we assume that the condition given by Eq. (4.33) is satisfied. It is noticed that $A_1(s)$ depends on the local gradient $\partial_r U_0|^{\pm}$. In Eq. (4.42), we need to hold the following relation to eliminate the term proportional to $A_1(s)$:

$$\hat{F}_+ = \hat{F}_-. \tag{4.43}$$

Finally, we obtain the Gibbs-Thomson relation at the first order

$$\bar{u}_0 + \varepsilon \tilde{U}_1 = -\kappa - \beta v_n, \tag{4.44}$$

where $\tilde{U}_1 = U_1|^+ = U_1|^-$ and

$$\beta = \alpha - \varepsilon[1 + (1-k)\bar{u}_0] \left(\frac{\tilde{K} + J\tilde{F}}{2J} \right). \tag{4.45}$$

From this relation, one can determine the kinetic coefficient τ or M within the thin-interface limit [8,12].

G. u equation at ε^0

Substituting the inner expansion of the u field into Eq. (4.9), we get the relation at order ε^0 and we integrate it once from 0 to η to find

$$q(\phi_0)\partial_\eta u_2 + q'(\phi_0)\phi_1 \partial_\eta u_1 + \kappa \int_0^{\eta} q(\phi_0)\partial_\xi u_1 d\xi$$

$$+ \int_0^{\eta} \frac{v_n[1 + k - (1-k)h(\phi_0)]}{2} \partial_\xi u_1 d\xi + v_n a(\phi_0)$$

$$\times [1 + (1-k)\bar{u}_0](\partial_\eta \phi_1) + v_n a'(\phi_0)\phi_1[1 + (1-k)\bar{u}_0]$$

$$\times (\partial_\eta \phi_0) + v_n a(\phi_0)[(1-k)u_1](\partial_\eta \phi_0)$$

$$+ \kappa v_n[1 + (1-k)\bar{u}_0] \int_0^{\eta} a(\phi_0)(\partial_\xi \phi_0) d\xi - \frac{v_n}{2}(1-k)$$

$$\times \int_0^{\eta} u_1 \partial_\xi h(\phi_0) d\xi - \frac{v_n}{2}[1 + (1-k)\bar{u}_0] h'(\phi)\phi_1$$

$$+ \partial_{ss} U_0 \int_0^{\eta} q(\phi_0) d\xi = A_3(s), \tag{4.46}$$

with constant $A_3(s)$. In the limit $\eta \to \pm\infty$, ϕ_1 and $\partial_\eta \phi_0$ become negligibly small values, we can drop the terms proportional to these quantities. The third term in Eq. (4.46) is expressed as

$$\kappa \int_0^{\eta} q(\phi_0)\partial_\xi u_1 d\xi = \kappa \left(\frac{1}{2} v_n' \int_0^{\eta} [h(\phi_0) - 2a(\phi_0)(\partial_\xi \phi_0)] d\xi \right.$$

$$\left. + A_1(s)\eta \right), \tag{4.47}$$

and the term proportional to $a(\phi_0)$ in the integrand cancels out with the eighth term in Eq. (4.46). Hence the sum of third and eighth terms yields

$$\kappa \left(\frac{1}{2} v_n' \int_0^{\pm\infty} h(\phi_0) d\xi + A_1(s)\eta \right)$$

$$= \mp \kappa \frac{v_n'}{2}\eta + \kappa \frac{v_n'}{2} \int_0^{\pm\infty} [h(\phi_0) - h(\mp 1)] d\xi + \kappa A_1(s)\eta$$

$$= \kappa q(\mp 1)\partial_r U_0|^{\pm}\eta + \kappa \frac{v_n'}{2} H_{\pm} \quad \text{as } \eta \to \pm\infty, \tag{4.48}$$

where we have used Eq. (4.28) and defined

$$H_{\pm} = \int_0^{\pm\infty} [h(\phi_0) - h(\mp 1)] d\xi. \tag{4.49}$$

The sum of the fourth and ninth terms leads to

$$\int_0^{\eta} \frac{v_n[1 + k - (1-k)h(\phi_0)]}{2} \partial_\xi u_1 d\xi$$

$$- \frac{v_n}{2}(1-k) \int_0^{\eta} u_1 \partial_\xi h(\phi_0) d\xi$$

$$= \frac{v_n[1 + k - (1-k)h(\phi_0)]}{2} u_1$$

$$= j_{\pm} v_n (U_1|^{\pm} + \eta \partial_r U_0|^{\pm}) \quad \text{as } \eta \to \pm\infty \tag{4.50}$$

with $j_+ = 1$, $j_- = k$. The eleventh term is rewritten as

$$\partial_{ss} U_0 \int_0^{\eta} q(\phi_0) d\xi = \partial_{ss} U_0 q(\mp 1)\eta + \partial_{ss} U_0 Q_{\pm} \quad \text{as } \eta \to \pm\infty, \tag{4.51}$$

where

$$Q_{\pm} = \int_0^{\pm\infty} [q(\phi_0) - q(\mp 1)] d\xi. \tag{4.52}$$

Regarding the first term in Eq. (4.46), the matching condition given in Eq. (4.11) leads to

$$\lim_{\eta \to \pm\infty} \partial_\eta u_2 = \partial_r U_1|^{\pm} + \eta \partial_r^2 U_0|^{\pm}. \tag{4.53}$$

As already discussed in Eq. (4.7), the outer solution of u field obeys the simple diffusion equation and this is expressed in the curvilinear coordinates as

$$q(\mp 1)\partial_r^2 U_{n'}|^{\pm} = -[j_{\pm} v_n + q(\mp 1)\kappa]\partial_r U_{n'}|^{\pm}$$

$$- q(\mp 1)\partial_s^2 U_{n'}|^{\pm}. \tag{4.54}$$

Substituting all the above expressions into Eq. (4.46), one can arrive at

$$q(\mp 1)\,\partial_r U_1|^{\pm} + j_{\pm} v_n\, U_1|^{\pm} + \kappa \frac{v_n'}{2} H_{\pm} + \partial_{ss} U_0 Q_{\pm} = A_3(s). \tag{4.55}$$

Thereby,

$$q(+1)\partial_r\, U_1|^{-} - q(-1)\partial_r\, U_1|^{+} = v_n(1-k)\tilde{U}_1 + \kappa \frac{v_n'}{2}(H_+ - H_-) + \partial_{ss} U_0 (Q_+ - Q_-). \tag{4.56}$$

In order to describe the mass conservation law within the accuracy of ε order, we require

$$H_+ = H_-, \tag{4.57}$$

$$Q_+ = Q_-. \tag{4.58}$$

If these relations are satisfied, one obtains

$$v_n[1 + (1-k)(\bar{u}_0 + \varepsilon \tilde{U}_1)] = q(+1)(\partial_r\, U_0|^{-} + \varepsilon \partial_r\, U_1|^{-}) - q(-1)(\partial_r\, U_0|^{+} + \varepsilon \partial_r\, U_1|^{+}). \tag{4.59}$$

H. Summary of the constraints

In the two-sided model, the description of the Gibbs-Thomson relation and the mass conservation law up to the first order in ε requires five types of integral constraints in the interpolating functions to be satisfied simultaneously. These constraints are summarized below.

The elimination of the discontinuity in u field requires [Eqs. (4.31) and (4.42)]

$$\int_0^{+\infty} \left(\frac{1}{q(\phi)} - \frac{1}{q(-1)} \right) d\eta = \int_0^{-\infty} \left(\frac{1}{q(\phi)} - \frac{1}{q(+1)} \right) d\eta, \tag{4.60}$$

$$\int_0^{+\infty} [p(\phi) - p(-1)] d\eta = \int_0^{-\infty} [p(\phi) - p(+1)] d\eta, \tag{4.61}$$

$$\int_0^{+\infty} \left(\frac{g(-1)}{q(-1)} - \frac{g(\phi)}{q(\phi)} \right) d\eta = \int_0^{-\infty} \left(\frac{g(+1)}{q(+1)} - \frac{g(\phi)}{q(\phi)} \right) d\eta. \tag{4.62}$$

The interface effects in the mass conservation law are removed when the following conditions are satisfied:

$$\int_0^{+\infty} [h(\phi) - h(-1)] d\eta = \int_0^{-\infty} [h(\phi) - h(+1)] d\eta, \tag{4.63}$$

$$\int_0^{+\infty} [q(\phi) - q(-1)] d\eta = \int_0^{-\infty} [q(\phi) - q(+1)] d\eta. \tag{4.64}$$

Equation (4.63) is related with the interface stretching effect and Eq. (4.64) is associated with surface diffusion, viz., solute diffusion along arclength of the interface. It should be noticed that we have only four degrees of freedom in choosing the relevant interpolating functions, viz., $h(\phi)$, $g(\phi)$, $q(\phi)$, and $a(\phi)$, while there are five types of constraints.

In the one-sided model, as detailed in Ref. [12], there are only three constraints, Eq. (4.61) with a modification in $p(\phi)$, Eqs. (4.63) and (4.64). Hence, thanks to the antitrapping current term, all the constraints can be satisfied. Especially, when one defines the following form of $a(\phi)$ [12]:

$$a(\phi) = \frac{[h(\phi) - 1][1 - q(\phi)]}{\sqrt{2}(\phi^2 - 1)}, \tag{4.65}$$

the constraint (4.61) becomes identical to Eq. (4.63) and, hence, one can determine $h(\phi)$ and $q(\phi)$, independently. On the other hand, in the two-sided model, if we choose a g function from one of the commonly used forms, we have only three functions at our disposal. Therefore, even though the antitrapping current term provides the additional degree of freedom in the model, it is quite difficult to fulfill all the requirements.

V. PHASE-FIELD MODELING FOR TWO-SIDED MODEL

It was demonstrated in the previous section that one needs to satisfy five types of constraints in the interpolating function in the thin-interface limit for the two-sided model. In this section, we present the form of the antitrapping current term which allows the elimination of the W-dependent interface effects with simple choice of the interpolating functions.

A. Antitrapping current term for two-sided model

From a closer look at the asymptotic analysis given in Sec. IV, it is realized that the integral constraints given in Eqs. (4.60) and (4.62) are associated with the constant $A_1(s)$ which is the integral constant for the expression of u_1. In the analysis for the one-sided model in Ref. [12], this constant is found to be proportional to v_n by utilizing the fact that $q(+1)=0$ in the one-sided model. In this study, we rewrite the spatial gradient of u field at the solid side of the interface as follows:

$$\partial_r U_0|^{-}(s) = -\tfrac{1}{2} v_n' \chi(s), \tag{5.1}$$

with a function $\chi(s)$. It is noted that this is not an assumption but a reexpression of $\partial_r U_0|^{-}$. Hence, Eq. (5.1) does not essentially change the asymptotic analysis. However, utilizing $\chi(s)$ function, we can express the constraints of the interpolating functions in different forms, which is advantageous in obtaining an appropriate form of the antitrapping current term. The dependence of χ on s is not explicitly specified in the discussion given below.

The above expression does not change the mathematical procedures and the results regarding ϕ equation at ε^0 (Sec. IV B), u equation at ε^{-2} (Sec. IV C) and ϕ equation at ε^1 (Sec. IV D). A difference appears in u equation at ε^{-1}. When Eq. (5.1) is substituted into Eq. (4.22), one obtains

$$\begin{aligned}\partial_\eta u_1 &= \left\{\tfrac{1}{2}v_n'[h(\phi_0) - 2a(\phi_0)(\partial_\eta\phi_0)] + A_1(s)\right\}/q(\phi_0)\\ &= \left[\tfrac{1}{2}v_n' + A_1(s)\right]/q(+1) = -\tfrac{1}{2}v_n'\chi \text{ as } \eta \to -\infty,\end{aligned} \tag{5.2}$$

and, accordingly,

$$A_1(s) = -\tfrac{1}{2}v_n'[1 + q(+1)\chi]. \tag{5.3}$$

Then, the expression of u_1 given by Eq. (4.23) is rewritten as

$$u_1 = \frac{1}{2}v_n'\int_0^\eta p'(\phi_0)d\xi + A_2(s), \tag{5.4}$$

where

$$p'(\phi_0) = \frac{[h(\phi_0) - 2a(\phi_0)(\partial_\xi\phi_0) - 1 - q(+1)\chi]}{q(\phi_0)}. \tag{5.5}$$

The matching condition yields

$$\begin{aligned}u_1 &= A_2(s) + \tfrac{1}{2}v_n'F_\pm' + \tfrac{1}{2}v_n'p'(\mp 1)\eta\\ &= U_1|^\pm + \eta\partial_r U_0|^\pm \text{ as } \eta \to \pm\infty,\end{aligned} \tag{5.6}$$

where

$$F_\pm' = \int_0^{\pm\infty}[p'(\phi_0) - p'(\mp 1)]d\eta. \tag{5.7}$$

Since the term proportional to $a(\phi_0)$ vanishes in the limit $\eta \to \pm\infty$, we have $p'(-1) = -[2 + q(+1)\chi]/q(-1)$ and $p'(+1) = -q(+1)\chi/q(+1)$. Therefore, we obtain

$$\begin{aligned}q(-1)\partial_r U_0|^+ &= -\tfrac{1}{2}v_n'[2 + q(+1)\chi],\\ q(+1)\partial_r U_0|^- &= -\tfrac{1}{2}v_n'q(+1)\chi,\end{aligned} \tag{5.8}$$

and we can again recover the mass conservation law within the leading order expression as given by Eq. (4.30). Moreover, we find the following relation from Eq. (5.6):

$$U_1|^+ - U_1|^- = \tfrac{1}{2}v_n'(F_+' - F_-'). \tag{5.9}$$

Hence, it is required to satisfy the following relation to remove the discontinuity of the u field across the interface:

$$F_+' = F_-' = \tilde{F}'. \tag{5.10}$$

It is important to note that there is only one integral constraint in this procedure, which is in contrast with the requirement of two constraints, (4.32) and (4.33), in the discussion of Sec. IV E.

Next we focus on ϕ equation at ε^2. The substitution of Eq. (5.4) into Eq. (4.36) leads to the expression for $A_2(s)$ and then, employing Eq. (5.6), one comprehends

$$U_1|^\pm = v_n'\left(\frac{\tilde{K}' + J\tilde{F}'}{2J}\right), \tag{5.11}$$

where

$$\tilde{K}' = \int_{-\infty}^{+\infty}\left[\int_0^\eta p'(\phi_0)d\xi\right]g'(\phi_0)\partial_\eta\phi_0 d\eta. \tag{5.12}$$

Hence, the condition of Eq. (4.62) is not required. We can again obtain the Gibbs-Thomson relation at the first order with the modification in definition of β as

$$\beta = \alpha - \varepsilon[1 + (1-k)\bar{u}_0]\left(\frac{\tilde{K}' + J\tilde{F}'}{2J}\right). \tag{5.13}$$

Finally, there is virtually no difference in the discussion concerning the u equation at ε^0 (Sec. IV G). It may be sufficient to point out only the following point. The third term in Eq. (4.46) is now expressed as

$$\begin{aligned}\kappa\int_0^\eta q(\phi_0)\partial_\xi u_1 d\xi = \frac{1}{2}v_n'\kappa\Bigg\{&\int_0^\eta [h(\phi_0) - 2a(\phi_0)(\partial_\xi\phi_0)]d\xi\\ &- [1 + q(+1)\chi]\eta\Bigg\}\end{aligned} \tag{5.14}$$

and, thus, the sum of the third and eighth terms yields

$$\begin{aligned}&\frac{1}{2}v_n'\kappa\left\{\int_0^\eta h(\phi_0)d\xi - [1 + q(+1)\chi]\eta\right\}\\ &= \frac{1}{2}v_n'\kappa\left\{\int_0^\eta [h(\phi_0) - h(\mp 1)]d\xi \mp \eta - [1 + q(+1)\chi]\eta\right\}\\ &= \kappa q(\mp 1)\partial_r U_0|^\pm\eta + \kappa\frac{v_n'}{2}H_\pm \text{ as } \eta \to \pm\infty,\end{aligned} \tag{5.15}$$

which is equivalent to Eq. (4.48). The other procedures are identical to those given in Sec. IV G and we obtain the mass conservation law (4.59) with the integral constraints, (4.63) and (4.64). It is important to note that in the above discussion, all the spurious interface effects vanish when one satisfies only three constraints (5.10), (4.63), and (4.64), which is quite comparable to the case of one-sided model [11,12].

We have not yet defined the specific form of $a(\phi)$. In this study, we focus on the following form:

$$a(\phi) = \frac{[h(\phi) - 1][1 - q(\phi)] - \chi[q(+1) - q(\phi)][1 - q(\phi)]}{\sqrt{2}(\phi^2 - 1)}, \tag{5.16}$$

with a given form of function χ. One may notice that when $\chi = 0$, Eq. (5.16) is reduced to the one given in Eq. (4.65). Importantly, the above definition of $a(\phi)$ leads to the following relation:

$$F_\pm' = H_\pm + \chi Q_\pm. \tag{5.17}$$

Thus, we have only two constraints $H_+ = H_-$ and $Q_+ = Q_-$, which allows to choose $h(\phi)$ and $q(\phi)$, independently. In this study, we choose

$$h(\phi) = \phi, \tag{5.18}$$

which is a computationally effective choice, satisfying $H_+ = H_-$ [8]. Also, we assume the following form for $q(\phi)$:

$$q(\phi) = \tfrac{1}{2}\{q(+1) + q(-1) + [q(+1) - q(-1)]\phi\}. \tag{5.19}$$

Then, the condition $Q_+ = Q_-$ becomes equivalent to $H_+ = H_-$ and hence all the constraints are satisfied. In this choice of the functions, $a(\phi)$ is given as

$$a(\phi) = \frac{1}{2\sqrt{2}}[1 - q(+1)]\Psi(\chi), \tag{5.20}$$

with

$$\Psi(\chi) = 1 - \tfrac{1}{2}[1 - q(+1)]\chi. \tag{5.21}$$

It is noted that when one takes $q(+1)=0$ and $\chi=0$, the Eq. (5.20) reads $a(\phi)=1/(2\sqrt{2})$ which is equivalent to the one proposed for the one-sided model [11,12]. On the other hand, when the symmetric model is concerned, i.e., $q(+1)=1$, $a(\phi)$ vanishes as is consistent with the model derived by Karma and Rappel for the symmetric case [8]. Therefore, the present model can be seen as a generalization of the quantitative phase-field models of two-limited cases, one-sided [11] and symmetric cases [8], into the two-sided case.

In the choice of the interpolating functions thus described, the kinetic coefficient β is expressed as

$$\beta = \alpha - \varepsilon[1 + (1-k)\bar{u}_0]\Psi(\chi)\left(\frac{K^* + JF^*}{2J}\right), \tag{5.22}$$

where K^* and F^* are given as

$$K^* = \int_{-\infty}^{+\infty}\left(\int_0^{\eta}\phi_0 d\xi\right)g'(\phi_0)\partial_\eta\phi_0 d\eta, \tag{5.23}$$

$$F^* = \int_0^{+\infty}(\phi_0 + 1)d\eta. \tag{5.24}$$

These are the same as the solvability integrals derived in the symmetric case [8]. In the dimensional units, Eq. (5.22) is rewritten as

$$\tilde{\beta} = a_1\frac{\tau}{\lambda^* W}\left\{1 - a_2\frac{\lambda^* W^2}{\tau D_l}[1 + (1-k)\bar{u}_0]\Psi(\chi)\right\}, \tag{5.25}$$

with

$$a_2 = \frac{K^* + JF^*}{2I}. \tag{5.26}$$

For the slow solidification process, the kinetic effect is negligibly small and, hence, $\tilde{\beta}$ is approximated to be zero. This is achieved for the symmetric case, $k=1$ and $q(+1)=1$ by holding $\tau = a_2 W^2\lambda^*/D_l$. For the two-sided case, the vanishing condition of the kinetic coefficient leads to

$$\tau = \frac{a_2 W^2\lambda^*}{D_l}[1 + (1-k)\bar{u}_0]\Psi(\chi). \tag{5.27}$$

This expression is identical to the one for the one-sided model [12], except for the term $\Psi(\chi)$ involved in Eq. (5.27). It is noted that the phase-field relaxation time τ depends on $\bar{u}_0$. This dependency is dealt with by assigning a constant value to $\bar{u}_0$ or by introducing u field dependence on τ as discussed in Refs. [12,13].

As described in this section, the antitrapping current term was determined for the system with arbitrary value of the solid diffusivity. Importantly, the present model contains the previously developed one-sided and symmetric phase-field models as special cases and, therefore, this model successfully bridges the gap between two limited cases. It should be pointed out that Eq. (5.20) and (5.27) involve the function $\chi(s)$ which is originally output quantity obtained from the simulation. In the present model, $\chi(s)$ is assumed to be a priori given quantity. The function $\chi(s)$ can be considered as an adjustable quantity of which value or form is numerically fixed by comparing the output with the other numerical solution for a certain (simple) condition. Also, the form of $\chi(s)$ can be assumed in terms of an approximate solution of the free-boundary problem. It is noted that the contribution of the antitrapping current term is proportional to W and hence, the result of the present model should be converged to a unique solution as W decreases regardless of the given form of $\chi(s)$, while the convergent behavior of the solution should depend on $\chi(s)$. In this regard, $\chi(s)$ can be considered as a quantity controlling the convergent behavior of the solution in this model. As demonstrated in Sec. VII, in fact, the convergent behavior with respect to W depend on the value of $\chi(s)$ and the solution of the present model becomes almost independent of the value of $\chi(s)$ when W is small.

B. Temperature dependence and anisotropy

In this study, our discussion has been directed to the isothermal solidification process. It is trivial to extend the present model to a directional solidification process within the frozen temperature approximation, in which the temperature field is given as

$$T(z) = T_0 + G(z - V_p t), \tag{5.28}$$

where G is temperature gradient along z axis and V_p is pulling speed. Then, the last term on the right-hand side of Eq. (3.10) $\lambda^* g'(\phi)u$ is replaced by $\lambda^* g'(\phi)[u + (z - V_p t)/l_T]$ with a thermal length $l_T = |m|(1-k)c_\infty/(GK)$ and the alloy concentration c_∞. This does not essentially change the final form of the antitrapping current term (5.20). For a more realistic simulation, one may solve heat conduction equation. The antitrapping current scheme for the one-sided model has been applied to the solidification process coupled with heat and solute diffusions in Ref. [13].

The crystalline anisotropy can be included in the standard manner. As is common practice, the orientation dependences are introduced to W and τ. These are described as $W(\theta) = W_0 a_s(\theta)$ and $\tau(\theta) = \tau_0 a_s(\theta)^2$ with $\theta = \arctan(\partial_y\phi/\partial_x\phi)$ and $a_s(\theta) = 1 + \varepsilon_4\cos(4\theta)$ for fourfold symmetry. Then, Eq. (3.10) is rewritten as

$$\tau(\theta)\partial_t\phi = \nabla[W(\theta)^2\nabla\phi] - \partial_x[W(\theta)W'(\theta)\partial_y\phi] + \partial_y[W(\theta)W'(\theta)\partial_x\phi] - f'(\phi) - \lambda^* g'(\phi)u, \tag{5.29}$$

where $W'(\theta)=dW/d\theta$. It is noted that the interface thickness W is involved in the antitrapping current term. As discussed in Ref. [12], since the anisotropy of the chemical capillary length $d_0[1-15\varepsilon_4\cos(4\theta)]$ is 15 times larger than the one of $W(\theta)$, it may be safe to use the mean value of $W(\theta)$ in the antitrapping current term which leads to only a small error.

VI. SUMMARY OF THE PRESENT MODELING

The essential equations of the present model are summarized in this section. We focus on isothermal solidification in dilute binary alloy system and, for simplicity, we do not take the crystalline anisotropy into account. The phase field ϕ specifies the solid phase with $\phi=+1$ and the liquid phase with $\phi=-1$. The time evolution of ϕ is described by

$$\tau\partial_t\phi = W^2\nabla^2\phi - f'(\phi) - \lambda^* g'(\phi)u, \tag{6.1}$$

where τ is the phase-field relaxation time, W is the measure of interface thickness and is related to the gradient energy coefficient, and λ^* is associated with the thermodynamic driving force. The interpolating functions were chosen so that $f'(\phi)=-\phi+\phi^3$ and $g'(\phi)=(1-\phi^2)^2$. In Eq. (6.1), u is the dimensionless concentration defined as $u=(c_l-c_l^e)/(c_l^e-c_s^e)$ with liquid concentration c_l, and equilibrium concentrations of liquid c_l^e and solid c_s^e. The time evolution of the conserved quantity u is given by the following diffusion equation:

$$\frac{[1+k-(1-k)h(\phi)]}{2}\partial_t u = \nabla[D_l q(\phi)\nabla u - j_{\mathrm{AT}}] + \frac{1}{2}[1+(1-k)u]\partial_t h(\phi), \tag{6.2}$$

where k is the partition coefficient and D_l is the liquid diffusivity. $h(\phi)$ and $q(\phi)$ are the interpolating functions. The antitrapping current j_{AT} is written as

$$j_{\mathrm{AT}} = -a(\phi)W[1+(1-k)u]\partial_t\phi\frac{\nabla\phi}{|\nabla\phi|}, \tag{6.3}$$

where $a(\phi)$ is the interpolating function. The thin-interface limit analysis demonstrated that precise description of the Gibbs-Thomson relation and mass conservation law at the interface imposes five constraints (4.60)–(4.64), on the interpolating functions. In order to avoid such restrictions on the model, we proposed the following form of $a(\phi)$,

$$a(\phi) = \frac{[h(\phi)-1][1-q(\phi)] - \chi[q(+1)-q(\phi)][1-q(\phi)]}{\sqrt{2}(\phi^2-1)}, \tag{6.4}$$

where χ is related to the concentration gradient at the solid side of the interface [Eq. (5.1)]. In this study, χ is employed as the parameter controlling the convergent behavior of the simulation result with respect to the interface thickness. When we define $h(\phi)=\phi$ and $q(\phi)=\{q(+1)+q(-1)+[q(+1)-q(-1)]\phi\}/2$, $a(\phi)$ is given as

$$a(\phi) = \frac{1}{2\sqrt{2}}[1-q(+1)]\Psi(\chi), \tag{6.5}$$

with

$$\Psi(\chi) = 1 - \tfrac{1}{2}[1-q(+1)]\chi. \tag{6.6}$$

Then, within the thin-interface limit model, the kinetic coefficient is expressed as

$$\tilde{\beta} = a_1\frac{\tau}{\lambda^* W}\left\{1 - a_2\frac{\lambda^* W^2}{\tau D_l}[1+(1-k)\bar{u}_0]\Psi(\chi)\right\}, \tag{6.7}$$

where $a_1=0.8839\cdots$ and $a_2=0.6267\cdots$ in the choice of interpolating functions described above [8]. $\bar{u}_0$ is constant related to u field profile. Furthermore, from the vanishing condition of the kinetic coefficient, one obtain

$$\tau = \frac{a_2 W^2\lambda^*}{D_l}[1+(1-k)\bar{u}_0]\Psi(\chi). \tag{6.8}$$

These are the essential equations for the present phase-field model. For the system with crystalline anisotropy, one has to solve Eq. (5.29) instead of Eq. (6.1). In the next section, the performance of this model is demonstrated.

VII. NUMERICAL RESULTS

In this section, the present model is subjected to the convergent test with respect to the interface thickness in order to investigate the computational performance. Our concern is placed on the isothermal dendrite growth process in two-dimensional system.

As pointed out in the Sec. V A, the computation of the present model requires a priori knowledge on $\chi(s)$. Within this model, the convergent behavior of the solution is considered to depend on the function form $\chi(s)$. In this regard, we consider the planner interface moving at a constant velocity v_n along r direction. An exact solution of Eqs. (4.1)–(4.3) for this problem is given by

$$u(r) = \begin{cases} [1-\beta v_n(1-k)]\exp(-v_n r) - 1 - k\beta v_n, & r>0, \\ -\beta v_n, & r<0 \end{cases} \tag{7.1}$$

and $k\beta v_n=\Omega-1$ with the far-field boundary condition $u(+\infty)=-\Omega$. Therefore, χ is given as $\chi=0$. For a general case, i.e., nonplanner interface, the value of χ deviates from zero, depending on the interface curvature. In this study, however, we assume that $\chi=0$ for simplicity. It will be seen that the present model demonstrates a reasonable convergent behavior even under this unsophisticated assumption. The effect of the χ value on the convergent behavior will be also demonstrated later.

Equations (6.2) and (5.29) were discretized based on standard second-order finite difference formulas with a square

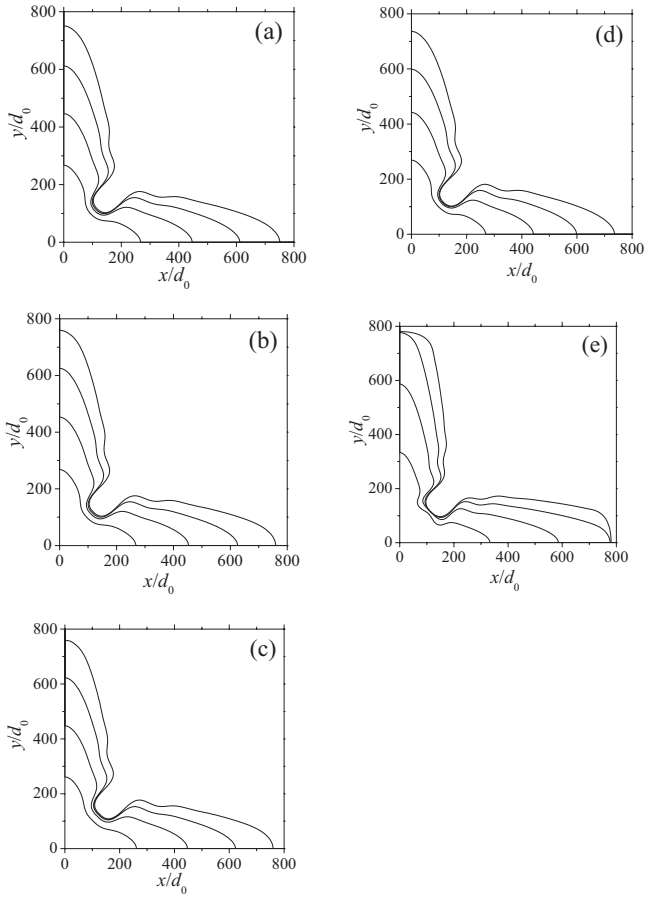

FIG. 1. Sequences of the dendrite growth patterns during isothermal solidification shown every interval of $D_l t/d_0^2=10\,000$, calculated by the present model with $\Omega=0.55$, $\varepsilon_4=0.02$, $k=0.15$, $D_s/D_l=0.1$, and (a) $d_0/W_0=0.40$, (b) $d_0/W_0=0.25$, and (c) $d_0/W_0=0.20$. The figures (d) and (e) represent the results obtained by a standard model without the antitrapping current term with $d_0/W_0=0.40$ and $d_0/W_0=0.25$, respectively.

gird spacing Δx. For the Laplacian of the phase field ϕ, we used a nine-point formula with the nearest and next-nearest neighbors, which reduces the grid anisotropy, as discussed in Refs. [8,12]. The time evolutions of ϕ and u fields were solved using a simple first-order Euler scheme. The simulations reported here were carried out with $\Delta x/W_0=0.4$ and $\Delta t/\tau_0=0.01$ by holding the relation $\tau_0=a_2\lambda^* {W_0}^2/D_l$, unless specified otherwise.

Our concern is first directed to a sequence of the dendrite growth patterns. We employed the system of a square shape with edge lengths of $x/d_0=y/d_0=800$ and imposed zero flux boundary condition along all the boundaries. The initial supersaturation $\Omega=0.55$ is uniformly assigned to all the gird points. The solidification started from a circular (quarter disk) seed of radius $r_s=20d_0$, located at corner of the system. The simulations were performed with $\varepsilon_4=0.02$, $k=0.15$, and $D_s/D_l=0.1$. The sequences of the dendrite growth processes are shown in Fig. 1, where $\phi=0$ contours are plotted with an interval of $D_l t/{d_0}^2=10\,000$. The figures (a)–(c) represent the results obtained from the present model with different values of d_0/W_0. One can see typical sequence of the dendrite growth pattern and, importantly, these sequences are almost

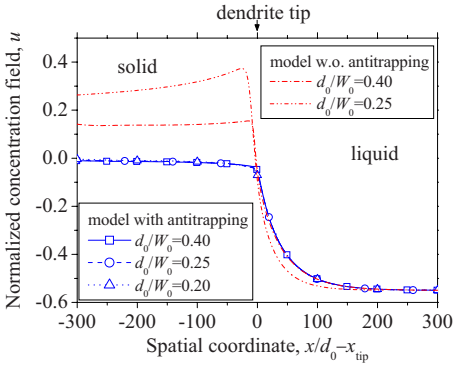

FIG. 2. (Color online) Normalized concentration u, field profile at $D_l t/d_0^2=20\,000$ along the central dendrite axis. The solid, dashed, and dotted lines are the results obtained by the present model, while the dashed-dotted and dashed-two dotted lines represent the results of the standard model. All the results of the present model are almost superimposed. For visual aid, one out of every 50 symbols along the profile is shown for the results of the present model.

independent of the value of d_0/W_0. Under a given set of the parameters, the solidification process is uniquely described by the present model within a certain range of d_0/W_0. For comparison, we performed the same simulation based on a standard model, viz., a model without the antitrapping current term and with a standard choice of $D(\phi)=[D_s+D_l+(D_s-D_l)\phi]/2$ and, hence, $q(\phi)=[D_s+D_l+(D_s-D_l)\phi][1+k+(1-k)\phi]/(4D_l)$, as is similar to the study in Ref. [11]. It is important to note that the standard model involves the spurious interface effects associated with the chemical potential jump at the interface and the surface diffusion. The results are demonstrated in Figs. 1(d) and 1(e). It is seen that the dendrite growth processes are substantially different depending on the value of d_0/W_0. The dendrite tip velocity increases with the increment of W_0, which is in marked contrast to the W_0-independent results obtained from the present model. The numerical simulation of the standard model becomes unstable at $d_0/W_0=0.20$ and we could not obtain the solution.

Figure 2 shows u field profile at $D_l t/{d_0}^2=20000$ along x direction at $y/d_0=0$ during the process shown in Fig. 1. The origin of the spatial coordinate was taken to be the position of dendrite tip x_{tip}. It is seen that the present model uniquely describes u field profile regardless of the value of d_0/W_0, while the results of the standard model are largely dependent on the value of d_0/W_0. Even at $d_0/W_0=0.4$, the standard model exhibits the solute trapping phenomena. From this comparison, one can comprehend that the u field profile is one of the sensitive measures for the convergence of the result with respect to d_0/W_0.

Next let us discuss the convergent behavior with respect to W_0. For these simulations, we employed a rectangular system with the edge lengths of $x/d_0=400$ and $y/d_0=800$. The solidification started from a circular seed of radius $r_s=20d_0$ at the corner of the system. We tracked the dendrite tip growing along the y direction by moving the calculation frame with a certain velocity in the $-y$ direction. This procedure allows us to describe the solidification process until the steady state is realized, within a reasonable computational

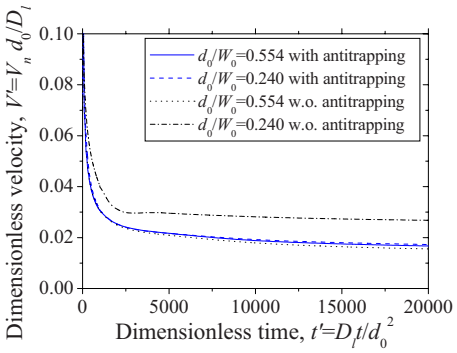

FIG. 3. (Color online) Temporal changes of the dendrite tip velocity. The results indicated by solid, dashed, and dotted lines are almost superimposed and the result of the present model is well converged even at $d_0/W_0=0.240$.

time. The temporal changes of the dendrite tip velocity are demonstrated in Fig. 3. These are the results obtained with $\Omega=0.55$, $\varepsilon_4=0.02$, $k=0.15$, and $D_s/D_l=0.1$. In all the cases, the dendrite tip velocity rapidly decreases in early time period and, then, keeps a constant value corresponding to the steady state value. The curves of the present model almost coincide with each other, indicating that the result at $d_0/W_0=0.24$ is well converged. On the other hand, the result of the standard model at $d_0/W_0=0.24$ is not converged. The steady state value of the standard model at $d_0/W_0=0.24$ is almost twice as large as the one at $d_0/W_0=0.554$.

The dendrite tip velocity at $D_l t/d_0^2=40000$, which can be considered to be the steady state velocity, is plotted with respect to W_0/d_0 in Fig. 4(a). The result of the standard model rapidly increases with increase in W_0/d_0. The stable solution could not be obtained with W_0/d_0 larger than 5.0. On the other hand, the present model demonstrates the well-converged behavior of the dendrite tip velocity even at relatively large value of $W_0/d_0=6.0$. Although the velocity of the present model gradually decreases with the increase in W_0/d_0, the convergent behavior is quite comparable to that of the symmetric model [8]. Figure 4(b) shows the dependence of the dendrite tip radius on W_0/d_0 at $D_l t/d_0^2=40\,000$. This well-converged behavior of the present model is also similar to the case in the symmetric model [8]. In Fig. 4(c), moreover, the concentration in solid at $40d_0$ away from the dendrite tip is plotted with respect to W_0/d_0. The present model demonstrates almost the constant value $c_s/c_l^e=0.15$. In contrast, the result of the standard model is not converged even at the smallest value employed here $W_0/d_0=1.8$, which may cause slight differences in the dendrite tip velocity and tip radius between the models at $W_0/d_0=1.8$. The convergent behavior was also studied for $D_s/D_l=0.5$ and the results are shown in Fig. 5. The other parameters in this simulation are the same as those used in the calculation of Fig. 4. It is again demonstrated that the convergent behavior obtained by the present model is excellent, as compared to that obtained by the standard model.

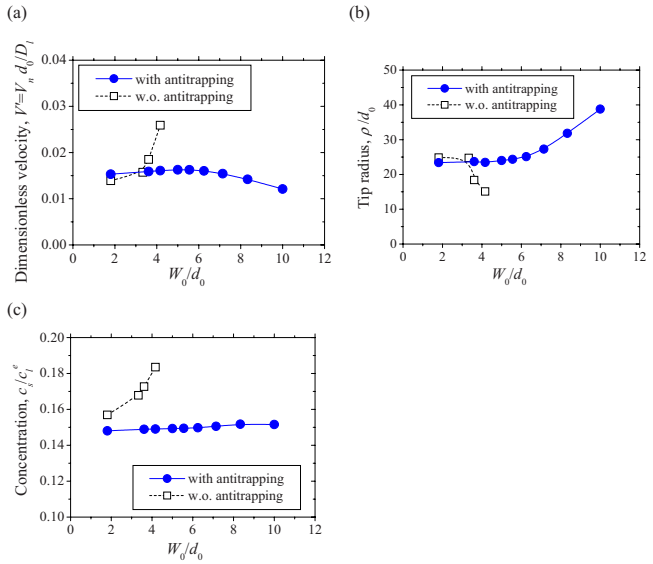

FIG. 4. (Color online) Convergent behavior of (a) dendrite tip velocity, (b) tip radius, and (c) concentration in solid at $40d_0$ away from the dendrite tip during steady state ($D_l t/d_0^2=40\,000$), calculated with $\Omega=0.55$, $\varepsilon_4=0.02$, $k=0.15$, $D_s/D_l=0.1$.

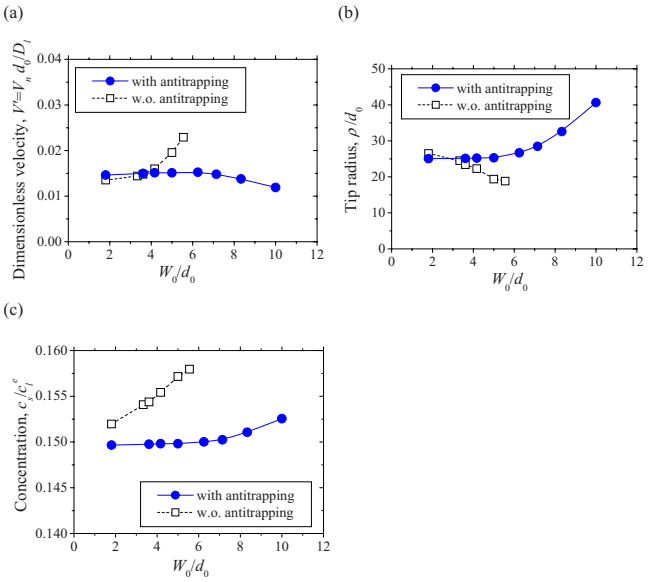

FIG. 5. (Color online) Convergent behavior of (a) dendrite tip velocity, (b) tip radius, and (c) concentration in solid at $40d_0$ away from the dendrite tip during steady state ($D_l t/d_0^2=40\,000$) calculated with $\Omega=0.55$, $\varepsilon_4=0.02$, $k=0.15$, $D_s/D_l=0.5$.

As already mentioned, the parameter (more precisely, the function) χ is regarded as the quantity controlling the convergent behavior in the present model. In the simulations discussed above, the quantity χ was taken to be zero. The dependence of the convergent behavior on the value of χ was investigated. The calculation parameters were chosen to be $\Omega=0.55$, $\varepsilon_4=0.02$, $k=0.15$, and $D_s/D_l=0.1$ and the relation $\tau_0=a_2\lambda^* W_0^2\Psi(\chi)/D_l$ was employed. Shown in Figs. 6(a) and 6(b) are the dependences of the dendrite tip velocity and the tip radius on the value of χ at $D_l t/d_0^2=60\,000$, respectively. When d_0/W_0 is small, the dendrite tip velocity increases and the tip radius decreases as the increase in χ. In the case of $d_0/W_0=0.554$, however, the velocity and tip radius are almost independent of the value χ. In other words, all the results are converged to the same value irrespective of

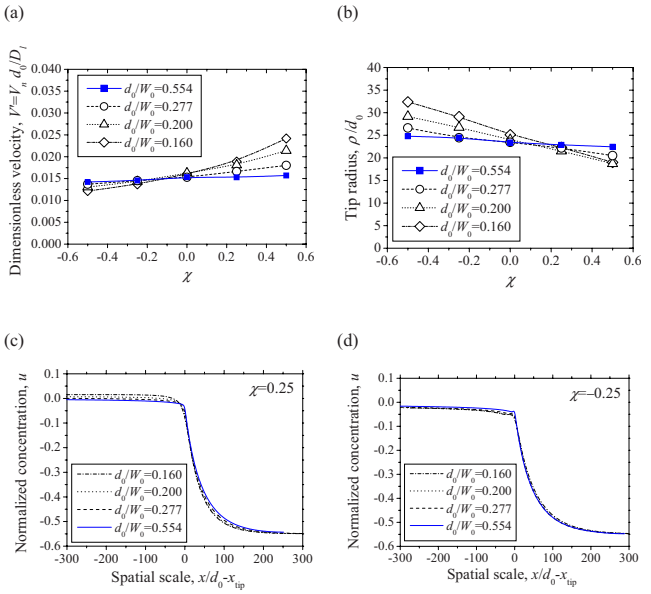

FIG. 6. (Color online) Dependence of (a) dendrite tip velocity, (b) tip radius at $D_l t/d_0^2=60\,000$ on value of χ calculated with $\Omega=0.55$, $\varepsilon_4=0.02$, $k=0.15$, $D_s/D_l=0.1$, and u field profiles along the central dendrite axis calculated with (c) $\chi=0.25$ and (d) $\chi=-0.25$.

the value of χ, as expected. The u field profiles in the vicinity of the dendrite tip calculated with $\chi=0.25$ and -0.25 are demonstrated in Figs. 6(c) and 6(d), respectively. χ is the quantity related to the concentration gradient at the solid side of the interface and, hence, the u field profile depends on the χ value. While the negative value of χ results in a kink at the interface [Fig. 6(d)], this kink becomes small as d_0/W_0 decreases. In Figs. 6(c) and 6(d), the u field profiles merge into a unique curve even at the different values of χ. Hence, χ can be recognized as the controlling parameter for the convergence and its appropriate value can be determined in the light of the convergent behavior. The physical meaning of χ is clear according to the discussion given in Sec. V A, which may enable a determination of the function form χ based on an analytical solution of the free-boundary problem for a certain simple case. Although such a function is expected to result in the excellent convergence, we considered in this study that the calculation with $\chi=0$ provides reasonable performance as is seen in Figs. 4 and 5.

As a benchmark test, we compare the result of the present model with the one from the linearized solvability theory. According to Barbieri and Langer [20], the following relation is held during the steady state in the limit of the small undercooling,

$$\rho^2 V_n \approx \frac{1+q(+1)}{2}(\rho^2 V_n)_{q(+1)=1}, \tag{7.2}$$

where $(\rho^2 V_n)_{q(+1)=1}$ indicates the quantity for the symmetric case. For this comparison, the simulations were performed with $\Omega=0.55$, $\varepsilon_4=0.02$, $k=1.0$, $d_0/W_0=0.277$, and $\chi=0$. Equation (6.2) was calculated by employing the value of $(\rho^2 V_n)_{q(+1)=1}$ obtained by the phase-field simulation. The result is demonstrated in Fig. 7. The agreement is quite reasonable, especially, in the range of small $q(+1)$. Although this agreement is not strong evidence supporting the accuracy of the present calculations, it is quite indicative of a wide range of applicability of the model to the system with arbitrary value of the solid diffusivity.

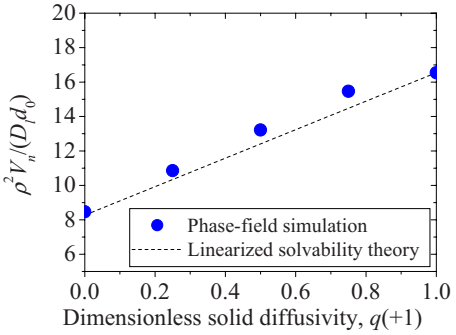

FIG. 7. (Color online) Comparison of dependence of $\rho^2 V_n$ on $q(+1)$ between the present model (solid circle) and the linearized solvability theory (dashed line). The calculations were performed with $\Omega=0.55$, $\varepsilon_4=0.02$, $k=1.0$, and $d_0/W_0=0.277$.

VIII. CONCLUSIONS

In this study, we extended the antitrapping current scheme devised in Ref. [11] to the isothermal solidification process of dilute binary alloy system involving the diffusion in solid. The present model is considered to be a generalized model based on the thin-interface limit in the light of the fact that the previously developed symmetric [8] and the one-sided [11] models are contained as special cases. For computation in practice, the present model requires *a priori* knowledge on the quantity χ which is originally output quantity from the simulation. The quantity χ is regarded as the parameter controlling the convergent behavior of the solution with respect to the interface thickness. Even at $\chi=0$ validated for the planner interface, the computations of the isothermal dendrite growth process demonstrated the reasonable convergent behavior comparable to that of the symmetric model [8]. It remains the possibility that the limitation on the interface thickness be further relaxed by a sophisticated choice of the value or function form of $\chi(s)$.

The diffusion in solid is of critical importance for accurate description of solidification phenomena covering the equilibrium to nonequilibrium processes such as Scheil-type solidification. The present model is applicable to the case with arbitrary value of the solid diffusivity, and hence, it can be utilized for analysis on a variety of the solidification processes in a wide range of binary alloy systems. The extension of the present model to multicomponent and multiphase systems remains to be one of the important tasks for a further development of the quantitative phase-field model.

ACKNOWLEDGMENTS

This work was partially supported by the Next Generation Super Computing Project, Nanoscience Program, MEXT, Japan.

[1] A. Karma, *Encyclopedia of Materials Science and Technology* (Elsevier, Oxford, 2001); L.-Q. Chen, Annu. Rev. Mater. Sci. **32**, 113 (2002); W. J. Boettinger, J. A. Warren, C. Beckermann, and A. Karma, *ibid.* **32**, 163 (2002); M. Ode, S. G. Kim and T. Suzuki, ISIJ Int. **41**, 1076 (2001).

[2] A. Jacot and M. Rappaz, Acta Mater. **50**, 1909 (2002); W. Wang, P. D. Lee, and M. McLean, *ibid.* **51**, 2971 (2003); J. A. Sethian and J. Strain, J. Comput. Phys. **98**, 231 (1992); R. Almgren, *ibid.* **106**, 337 (1993).

[3] R. Kobayashi, Physica D **63**, 410 (1993); G. B. McFadden, A. A. Wheeler, R. J. Braun, S. R. Coriell, and R. F. Sekerka, Phys. Rev. E **48**, 2016 (1993); A. A. Wheeler, B. T. Murray, and R. J. Schaefer, Physica D **66**, 243 (1993); S.-L. Wang, R. F. Sekerka, A. A. Wheeler, B. T. Murray, S. R. Coriell, R. J. Braun, and G. B. McFadden, *ibid.* **69**, 189 (1993).

[4] A. A. Wheeler, W. J. Boettinger, and G. B. McFadden, Phys. Rev. A **45**, 7424 (1992); A. A. Wheeler, W. J. Boettinger, and G. B. McFadden, Phys. Rev. E **47**, 1893 (1993); A. Karma, *ibid.* **49**, 2245 (1994); J. A. Warren and W. J. Boettinger, Acta Metall. Mater. **43**, 689 (1995).

[5] I. Steinbach, F. Pezzola, B. Nestler, M. Seeßelberg, R. Prieler, G. J. Schmitz and J. L. L. Rezende, Physica D **94**, 135 (1996); J. Tiaden, B. Nestler, H. J. Diepers and I. Steinbach, *ibid.* **115**, 73 (1998); I. Steinbach and F. Pezzolla, *ibid.* **134**, 385 (1999); B. Neslter, A. A. Wheeler, and H. Gracke, Comput. Mater. Sci. **26**, 111 (2003); S. G. Kim, W. T. Kim, T. Suzuki, and M. Ode, J. Cryst. Growth **261**, 38 (2004); B. Boettger, J. Eiken, and I. Steinbach, Acta Mater. **54**, 2697 (2006); R. S. Qin, E. R. Wallach, and R. C. Thomson, J. Cryst. Growth **279**, 163 (2005); J. Eiken, B. Bottger, and I. Steinbach, Phys. Rev. E **73**, 066122 (2006).

[6] G. Caginalp, Phys. Rev. A **39**, 5887 (1989).

[7] S.-L. Wang and R. F. Sekerka, Phys. Rev. E **53**, 3760 (1996).

[8] A. Karma and W.-J. Rappel, Phys. Rev. E **53**, R3017 (1996); **57**, 4323 (1998).

[9] S. G. Kim, W. T. Kim, and T. Suzuki, Phys. Rev. E **60**, 7186 (1999).

[10] R. F. Almgren, SIAM J. Appl. Math. **59**, 2086 (1999).

[11] A. Karma, Phys. Rev. Lett. **87**, 115701 (2001).

[12] B. Echebarria, R. Folch, A. Karma, and M. Plapp, Phys. Rev. E **70**, 061604 (2004).

[13] J. C. Ramirez, C. Beckermann, A. Karma, and H.-J. Diepers, Phys. Rev. E **69**, 051607 (2004).

[14] M. Greenwood, M. Haataja, and N. Provatas, Phys. Rev. Lett. **93**, 246101 (2004); C. W. Lan and C. J. Shih, Phys. Rev. E **69**, 031601 (2004); J. C. Ramirez and C. Beckermann, Acta Mater. **53**, 1721 (2005); A. Badillo and C. Beckermann, *ibid.* **54**, 2015 (2006); C. Tong, M. Greenwood, and N. Provatas, Phys. Rev. B **77**, 064112 (2008).

[15] R. Folch and M. Plapp, Phys. Rev. E **68**, 010602(R) (2003); **72**, 011602 (2005); H. Emmerich and R. Siquieri, J. Phys.: Condens. Matter **18**, 11121 (2006); M. Plapp, J. Cryst. Growth **303**, 49 (2007); R. Siquieri and H. Emmerich, Philos. Mag. Lett. **87**, 829 (2007).

[16] S. G. Kim, Acta Mater. **55**, 4391 (2007).

[17] W. Kurz and D. J. Fisher, *Fundamentals of Solidification* (Trans Tech, Aedermannsdorf, Switzerland, 1992).

[18] A. Gopinath, R. C. Armstrong, and R. A. Brown, J. Cryst. Growth **291**, 272 (2006).

[19] R. Folch, J. Casademunt, A. Hernández-Machado, and L. Ramírez-Piscina, Phys. Rev. E **60**, 1724 (1999); K. R. Elder, M. Grant, N. Provatas, and J. M. Kosterlitz, *ibid.* **64**, 021604 (2001).

[20] A. Barbieri and J. S. Langer, Phys. Rev. A **39**, 5314 (1989).